Biomimetic Control Based on a Model of Chemotaxis in *Escherichia coli*

Toshio Tsuji*,**
Hiroshima University

Michiyo Suzuki**,†
Hiroshima University

Noboru Takiguchi‡,§
Hiroshima University

Hisao Ohtake¶
Osaka University

Abstract In the field of molecular biology, extending now to the more comprehensive area of systems biology, the development of computer models for synthetic cell simulation has accelerated extensively and has begun to be used for various purposes, such as biochemical analysis. These models, describing the highly efficient environmental searching mechanisms and adaptability of living organisms, can be used as machine-control algorithms in the field of systems engineering. To realize this biomimetic intelligent control, we require a stripped-down model that expresses a series of information-processing tasks from stimulation input to movement. Here we selected the bacterium *Escherichia coli* as a target organism because it has a relatively simple molecular and organizational structure, which can be characterized using biochemical and genetic analyses. We particularly focused on a motility response known as chemotaxis and developed a computer model that includes not only intracellular information processing but also motor control. After confirming the effectiveness and validity of the proposed model by a series of computer simulations, we applied it to a mobile robot control problem. This is probably the first study showing that a bacterial model can be used as an autonomous control algorithm. Our results suggest that many excellent models proposed thus far for biochemical purposes can be applied to problems in other fields.

Keywords
Bacterial chemotaxis, bacterial motor control, computer simulation, biomimetic control, mobile robot control

1 Introduction

The development of synthetic cell simulation software [22] has accelerated greatly in recent years and has begun to be used for various purposes, such as the analysis of biochemical responses. It is effective to focus on a protozoan and a unicellular organism as the target of the modeling study,

* Contact author.
** Department of Artificial Complex Systems Engineering, Graduate School of Engineering, Hiroshima University, 1-4-1 Kagamiyama, Higashi-Hiroshima, Japan. E-mail: tsuji@bsys.hiroshima-u.ac.jp (T.T.)
† Present address: Microbeam Radiation Biology Group, Quantum Beam Science Directorate, Japan Atomic Energy Agency, 1233 Watanuki-machi, Takasaki, Japan. E-mail: michiyosuzuki@ieee.org
‡ Department of Molecular Biotechnology, Graduate School of Advanced Sciences of Matter, Hiroshima University, 1-3-1 Kagamiyama, Higashi-Hiroshima, Japan.
§ Present address: School of Natural Systems, College of Science and Engineering, Kanazawa University, Kakuma-machi, Kanazawa, Japan. E-mail: ntaki@t.kanazawa-u.ac.jp
¶ Department of Biotechnology, Graduate School of Engineering, Osaka University, 2-1 Yamada-oka, Suita, Japan. E-mail: hohtake@bio.eng.osaka-u.ac.jp

because the outcome of information processing within a cell body can be studied from its movement. In fact, although bacteria have the simplest molecular structure and organization of all free-living organisms, they can still change their swimming direction autonomously, depending on environmental stimuli. In addition, they have an adaptation mechanism for detecting new environmental stimuli when identical stimuli continue to be present and they lack reactions or can ignore such continuous stimuli. Such autonomous and adaptive behavior, which allows bacteria to accumulate around attractants and escape from repellents, is generally termed chemotaxis [4, 5, 13, 15, 18, 20, 24, 25]. It is interesting to note that in chemotaxis the intracellular information processed from stimulus reception to motor control is achieved by the involvement of several proteins. Bacteria achieve information processing corresponding to various stimuli by effectively using limited amounts of these molecular components.

Several computer models have been developed that deal with bacterial chemotaxis [4, 5, 13, 15, 18, 20, 24, 25] or adaptation [19, 26]. In particular, E-CELL [27, 33, 34] is a representative software system that deals with *Escherichia coli* as a target organism. This software has enabled simulation of the metabolic system. Additionally, Bray et al. [6–10] have presented computer models to reproduce an intracellular information process identical to that in an actual living bacterium. Hauri and Ross [12] constructed a model based on the adaptation mechanism. Barkai and Leibler [1] reported that the adaptation mechanism of bacterial chemotaxis is robust and is represented as a biochemical network of interactions. Hazelbauer [14] developed a program that incorporates both spatial locations of protein components and diffusion of the components within a cell and conducted a series of simulations focusing on the distribution of protein components.

From the systems engineering viewpoint, a model of an organism that includes such excellent environmental searching mechanisms and adaptability can be considered as a machine control algorithm. The most important difference of such a biomimetic algorithm from a conventional algorithm is that it does not require the user to program in detail appropriate instructions for each possible occasion. That is, the machine can behave well even in unknown environments by using an organism-like flexible information-processing algorithm. Biomimetic control may enable us to reduce the programming cost, and this is considered a great benefit in machine control. Therefore, here we will consider a method for biomimetic intelligent control. Nevertheless, to achieve this biomimetic control, we do not require a detailed model such as previous network system models containing hundreds of components and specialized for stages of information processing. Rather, we present a stripped-down model that expresses a series of information-processing tasks from stimulation input to movement. Therefore, in this study we constructed a simple model of *E. coli* based on the entire signal transduction process from external stimuli input to the motion signal for the flagellum motor.

This exercise facilitated the development of a bacterial model for the computer simulation of chemotaxis. The results of these simulations were then compared with the chemotactic behavior of *E. coli* in vivo to demonstrate the effectiveness and validity of the proposed computer model. Finally, the proposed model was applied to a motor control problem for mobile robots and showed that the chemotactic algorithm of the bacterial cell could be used successfully to achieve that kind of behavior in mobile robots.

2 Bacterial Chemotaxis and Signal Transduction

2.1 Bacterial Chemotaxis

E. coli has several spiral flagella, whose length is several times that of the bacterium (approximately 2 μm long). It regulates flagellar rotation to swim toward regions with a high concentration of chemoattractants. During swimming, a driving force is generated as the flagella rotate in the counterclockwise direction, whereas in the tumbling state the flagella rotate in the clockwise direction, causing bacteria to tumble, or gyrate randomly [2]. Moreover, because these microorganisms are small, they also show random movements from the effects of Brownian motion.

Bacteria can detect the spatial gradients of chemoattractants by monitoring their change in concentration. Chemotaxis is the process by which bacteria migrate through the concentration gradients

of chemoattractants and repellents. This is a rapid process that occurs within 1 s after the cells have been subjected to a chemical stimulus. Chemotaxis has assumed a special role in providing insight into the intracellular signal transduction network of simple living organisms. Computer-assisted capillary techniques [3, 21] have been developed to measure bacterial chemotaxis. In these methods, digital image processing is used to determine the number of bacterial cells accumulating around the mouth of a capillary that contains the chemical compound under test, embedded in agarose gel. Bacteria can also adapt to the continued presence of an environmental stimulus (adaptation) [19, 26]. This is an important process for the detection of new environmental stimuli.

2.2 Molecular Signal Transduction in the Bacterial Cell

Figure 1 shows a schematic illustration of chemotactic signal transduction in *E. coli*. First, sensors on the cell surface receive environmental stimuli, and these are then converted to internal signals by chemotactic transducers, which can also sense various types of chemical stimuli directly. After amplification and integration, the internal signals are transmitted through the intracellular signal transduction pathway to the flagellar motors. The components of this pathway are regulated by phosphorylation and dephosphorylation of proteins, and they act by chemical diffusion between the proteins [20].

A transducer allows the cells to modulate their behavior in response to external stimuli. Seven states are recognized : [I], [II], [III], [IV], [II′], [III′], and [IV′] as shown in Figure 1. State [I] is the initial state of the transducer, and its intracellular structure is transformed to [II] → [III] → [IV] by binding of the chemoattractant (Atr in the figure). There are reversible responses in the [I] → [II] and [III] → [IV] transformations. On the other hand, when a chemical repellent (Rpl in the figure) binds to the transducer in the initial state [I], the transformation progresses as [II′] → [III′] → [IV′]. External signals are transmitted to the intracellular chemotaxis proteins via a chain of these structural transformations [14, 24, 26].

The intracellular signal transduction pathway involves at least five chemotactic proteins: CheY, CheZ, CheA, CheB, and CheW [4, 20]. When the transducer receives signal information regarding

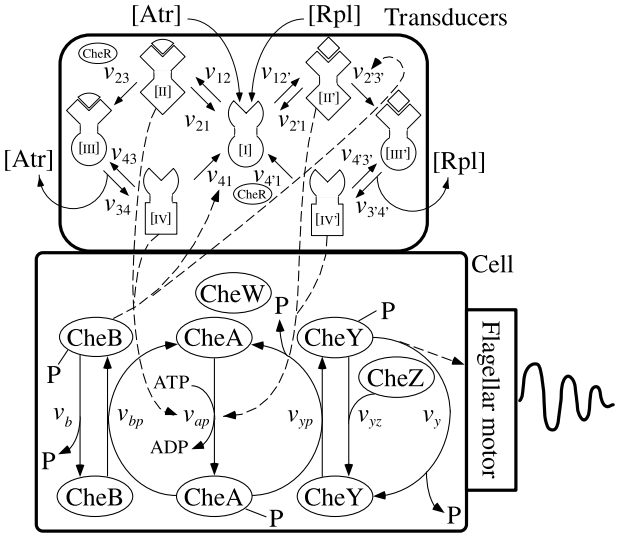

Figure 1. Schematic of chemotactic signal transduction in *E. coli*. Sensors on the cell surface receive environmental stimuli, and the stimulation signals are then converted to internal signals by chemotactic transducers. After amplification and integration, the internal signals are transmitted through the intracellular signal transduction pathway to the flagellar motors. The transducer allows the cells to modulate their behavior in response to external stimuli. It has seven states: [I], [II], [III], [IV], [II′], [III′], and [IV′], encoded by the chemotaxis genes. The solid lines in this figure show chemical reactions. It should be noted that the coefficients indicated by the arrows with the dashed lines change depending on the concentrations of the corresponding transducer states and proteins in the cell body.

an environmental stimulus, it forms a complex with CheW and converts the external signals to internal signals through the phosphorylation and dephosphorylation of CheA. There are two pathways for intracellular signal transduction starting from phosphorylated CheA (CheA-P in the figure). The first originates from the flagellar motor via CheY. In the CheY → CheY-P response, the bacterial cell tends to assume the swimming state when the concentration of CheY-P is low, and the tumbling state when the concentration of CheY-P is high. Therefore, it can be considered that the ratio of the concentrations of CheY and CheY-P function as a command signal to the flagellar motor. The second pathway that is initiated via CheB is used to provide intracellular information feedback to the transducer. These two pathways are controlled by the transducers [II], [II′], [IV], and [IV′]. The dephosphorylation of CheA is accelerated in states [II] and [IV′], whereas the phosphorylation of CheA is accelerated in states [IV] and [II′]. As a result, the ratio of CheY to CheY-P changes, thereby modulating bacterial behavior.

These signal transductions are performed rapidly; the response of a bacterial cell to chemoattractants is typically observed within 1 s after stimulus reception. In one constructed model, the time required for intracellular signal transduction was observed to be approximately 0.2 s [19].

3 Description of a Model of the Bacterial Motor Control System

The proposed model consists of the following three components: (1) a transducer component that senses chemical concentrations in the environment and transmits external signals to the cell body, (2) an intracellular signal network component that calculates commands to the flagellar motor according to the signals, and (3) a flagellar motor control component that determines the swimming direction.

3.1 Transducer Component

Based on molecular evidence [15, 24], because the transducer exhibits seven states, [I] through [IV] and [II′] through [IV′] as shown in Figure 1, the transformation of the states is represented by the following equations:

$$\dot{C}_1(t) = v_{41}(t)C_4(t) + v_{4'1}C_{4'}(t) + v_{21}C_2(t) + v_{2'1}C_{2'}(t) - \{v_{12}C_{\mathrm{atr}}(t) + v_{12'}C_{\mathrm{rpl}}(t)\}C_1(t), \tag{1}$$

$$\dot{C}_2(t) = v_{12}C_1(t)C_{\mathrm{atr}}(t) - v_{21}C_2(t) - v_{23}C_2(t), \tag{2}$$

$$\dot{C}_3(t) = v_{23}C_2(t) - v_{34}C_3(t) + v_{43}C_4(t)C_{\mathrm{atr}}(t), \tag{3}$$

$$\dot{C}_4(t) = v_{34}C_3(t) - v_{43}C_4(t)C_{\mathrm{atr}}(t) - v_{41}(t)C_4(t), \tag{4}$$

$$\dot{C}_{2'}(t) = v_{12'}C_1(t)C_{\mathrm{rpl}}(t) - v_{2'1}C_{2'}(t) - v_{2'3'}(t)C_{2'}(t), \tag{5}$$

$$\dot{C}_{3'}(t) = v_{2'3'}(t)C_{2'}(t) - v_{3'4'}C_{3'}(t) + v_{4'3'}C_{4'}(t)C_{\mathrm{rpl}}(t), \tag{6}$$

$$\dot{C}_{4'}(t) = v_{3'4'}C_{3'}(t) - v_{4'3'}C_{4'}(t)C_{\mathrm{rpl}}(t) - v_{4'1}C_{4'}(t), \tag{7}$$

where $C_i(t) \geq 0$ [$i \in (1, 2, 3, 4, 2', 3', 4')$] are the concentrations in each state at time t. Note that the Arabic numerals here correspond to the states that are shown in Roman numerals, such as [I] and [I′]. Here $C_{\mathrm{atr}}(t) \geq 0$ and $C_{\mathrm{rpl}}(t) \geq 0$ are the concentrations of the chemoattractants and repellents, respectively, and v_{12}, v_{21}, v_{23}, v_{34}, v_{43}, $v_{12'}$, $v_{2'1}$, $v_{3'4'}$, $v_{4'3'}$, and $v_{4'1}$ (≥ 0) are the invariable coefficients of the transformation reaction from state [i] to state [j] [$i \neq j \in (1, 2, 3, 4, 2', 3', 4')$]. The initial concentration of state [I] is set as $C_1(0) = 5$ μM. As initially all transducers are in state [I], the initial value of each concentration can be given as $C_2(0) = C_3(0) = C_4(0) = C_{2'}(0) = C_{3'}(0) = C_{4'}(0) = 0$ μM.

The transducer acts on itself according to the type of chemical stimulus and decodes the external information regarding the concentrations of the stimulus in each state. The variable coefficients of the transformation reaction are $v_{41}(t)$ and $v_{2'3'}(t)$, and they are assumed to be in proportion to the

concentrations of phosphorylated CheB (CheB-P), $C_{bp}(t)$. These are respectively defined by the following equations:

$$v_{41}(t) = f_{41} C_{bp}(t), \tag{8}$$

$$v_{2'3'}(t) = f_{2'3'} C_{bp}(t), \tag{9}$$

where f_{41} and $f_{2'3'}$ (≥ 0) are invariable coefficients.

3.2 Intracellular Signal Network Component

Because intracellular signals are processed by chemical reactions among proteins in the cell body such as CheA and CheB, the reactions can be expressed by the following state equations:

$$\dot{C}_{ap}(t) = v_{ap}(t) C_a(t) - \{v_{yp}(t) C_y(t) + v_{bp}(t) C_b(t)\} C_{ap}(t), \tag{10}$$

$$\dot{C}_{yp}(t) = v_{yp}(t) C_y(t) C_{ap}(t) - v_{y\zeta} C_{yp}(t) C_\zeta(t) - v_y C_{yp}(t), \tag{11}$$

$$\dot{C}_{bp}(t) = v_{bp}(t) C_b(t) C_{ap}(t) - v_b C_{bp}(t), \tag{12}$$

$$\dot{C}_a(t) = v_{yp}(t) C_y(t) C_{ap}(t) + v_{bp}(t) C_b(t) C_{ap}(t) - v_{ap}(t) C_a(t), \tag{13}$$

$$\dot{C}_y(t) = v_{y\zeta} C_{yp}(t) C_\zeta(t) + v_y C_{yp}(t) - v_{yp}(t) C_y(t) C_{ap}(t), \tag{14}$$

$$\dot{C}_b(t) = v_b C_{bp}(t) - v_{bp}(t) C_b(t) C_{ap}(t), \tag{15}$$

where $C_a(t)$, $C_{ap}(t)$, $C_b(t)$, $C_{bp}(t)$, $C_y(t)$, $C_{yp}(t)$, and $C_\zeta(t)$ are the chemical concentrations of the proteins CheA, CheA-P, CheB, CheB-P, CheY, CheY-P, and CheZ, respectively, and v_b, v_y, and $v_{y\zeta}$ (≥ 0) are the invariable coefficients of the reactions between the proteins. The variable coefficient $v_{ap}(t)$ for the signal input from the transducer is defined using the concentrations in states [II] and [IV] as follows:

$$v_{ap}(t) = f_{ap} C_4(t) + f'_{ap} C_{2'}(t) - f_a C_2(t) - f'_a C_{4'}(t) + k_{ap}, \tag{16}$$

where f_{ap}, f'_{ap}, f_a, and f'_a are invariable coefficients and k_{ap} is an invariable coefficient with respect to the phosphorylation of CheA. The variable coefficients $v_{bp}(t)$ and $v_{yp}(t)$ are assumed to be in proportion to the concentration of CheA-P [i.e., $C_{ap}(t)$] and are defined respectively as follows:

$$v_{bp}(t) = f_{bp} C_{ap}(t), \tag{17}$$

$$v_{yp}(t) = f_{yp} C_{ap}(t), \tag{18}$$

where f_{bp} and f_{yp} (≥ 0) are invariable coefficients.

3.3 Flagellar Motor Control Component

The rotational direction of the flagellar motor is determined by $d(t)$, which is calculated from the CheY-P concentration $C_{yp}(t)$ as follows [8]:

$$d(t) = 1 - \frac{C_{yp}(t)^h}{2.333(SetC_{yp}(t))^h + C_{yp}(t)^h}, \tag{19}$$

where $SetC_{yp}(t)$ is the CheY-P concentration under the unstimulated state in wild bacteria, and the Hill coefficient h is set at 5.5 [8]. When $SetC_{yp}(t)$ is set at 1.63 μM, based on previous literature [8], $d_0(t)$, the resulting $d(t)$ in the unstimulated state, where $C_{yp}(t) = SetC_{yp}(t)$, is approximately 0.6988. Under this condition, the bacteria typically tend to be in the swimming state when $d(t) \geq d_0(t)$, whereas they tend to be in the tumbling state when $d(t) < d_0(t)$ [10]. Therefore, $d(t)$ decreases with an increase in $C_{yp}(t)$, and the probability of the tumbling state increases. Likewise, $d(t)$ increases with a decrease in $C_{yp}(t)$, and the probability of the swimming state increases. The direction of the flagellar rotation is determined using the time constant T_s, and the swimming velocity v is set appropriately. Additionally, in the tumbling state, the value of v is set at 0 μm/s.

The bacterium cannot always swim straight, and the swimming direction of the cell can change by 27 deg on average from the current direction [2] (see Figure 2). The swimming direction changes considerably during tumbling. In the computer model, the swimming direction was expressed using a conic bus bar in which the conic central axis corresponded to the vector of the current swimming direction and this was changed randomly by the uniform distribution.

3.4 Environmental Model

A bacterium is capable of detecting the spatial gradients of chemicals during its movement. These gradients in the environment can be expressed by the diffusion equation [2]. In an environment containing a sufficient concentration of chemicals, $C_{atr}(r)$ and $C_{rpl}(r)$ depend only on the distance from the center of the chemical concentration, and they converge exponentially. In the simulation study, chemical concentration gradients of attractants and repellents, $C_{atr}(r)$ and $C_{rpl}(r)$, respectively, are derived using one of the following two equations based on the diffusion equation:

$$C_{\text{cent\_high}}(r) = \begin{cases} \frac{I}{4\pi D r_{\text{near}}} & (r < r_{\text{near}}), \\ \frac{I}{4\pi D r} & (r_{\text{near}} \leq r \leq r_{\text{far}}), \\ 0 & (r > r_{\text{far}}), \end{cases} \tag{20}$$

$$C_{\text{cent\_low}}(r) = \begin{cases} 0 & (r < r_{\text{near}}), \\ \frac{I}{4\pi D}\left(\frac{1}{r_{\text{near}}} - \frac{1}{r}\right) & (r_{\text{near}} \leq r \leq r_{\text{far}}), \\ \frac{I}{4\pi D r_{\text{near}}} & (r > r_{\text{far}}), \end{cases} \tag{21}$$

where $C_{\text{cent\_high}}(r)$ in Equation 20 expresses the chemical environment, so that the concentration of chemicals increases toward the center of the gradient: that is, the center is in a high-concentration area

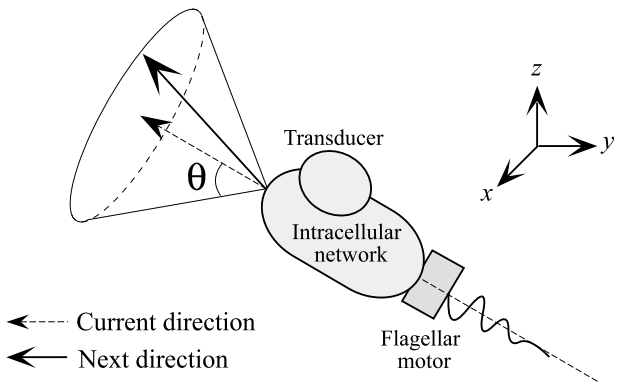

Figure 2. Change in the direction of motion. The swimming direction is expressed using a conic bus bar in which the conic central axis corresponds to the vector of the present swimming direction, and it is changed randomly with a uniform distribution. In the simulation, the angle θ between the conic central axis and the bus bar was set at 27 deg during swimming and 103 deg during tumbling.

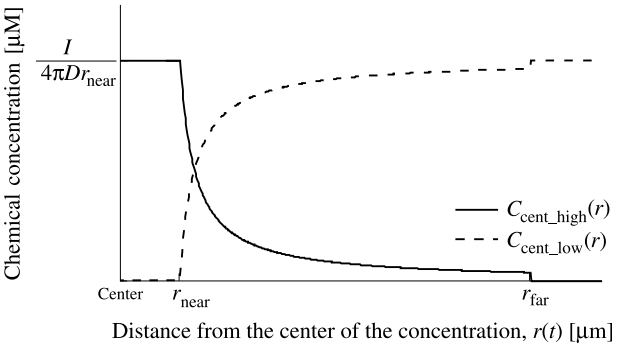

Figure 3. Chemical concentration gradients calculated by Equations 20 and 21. The solid line indicates the concentration gradient given by Equation 20, and the dashed line indicates that given by Equation 21. In our simulation, concentration gradients of attractants and repellents, $C_{atr}(r)$ and $C_{rpl}(r)$, respectively, are given by Equation 20 or 21.

(the solid line in Figure 3). $C_{cent\_low}(r)$ in Equation 21 expresses the environment in which the center is in a low-concentration area (the dashed line in Figure 3). In both equations, I is the chemical input per unit time, and D is the diffusion coefficient; here we take $I = 5.027 \times 10^{-9}$ μM/s and $D = 1 \times 10^{-3}$ mm^2/s. Finally, r indicates the distance from the concentration center, and r_{near} and r_{far} are two threshold values. The former is close to the center of the chemical concentration. $C_{atr}(t)$ in Equations 1–4 and $C_{rpl}(t)$ in Equations 5–7 are calculated using Equation 20 or 21, depending on $r(t)$, which is the distance at time t. To be brief, $C_{atr}(t)$ and $C_{rpl}(t)$ indicate $C_{atr}(r)$ and $C_{rpl}(r)$ at t.

In the next section, we show computer simulations of bacterial chemotaxis under virtual chemical environments given by Equation 20 and/or Equation 21.

4 Chemotactic Behavior of Virtual Bacteria

Because the proposed model is expressed using complex nonlinear differential equations, it is difficult to evaluate its behavior analytically. In addition, most of the coefficients in the system are unknown, because they cannot be measured by electrophysiological methods commonly used in molecular biology. Therefore, to perform chemotactic simulations with the proposed model, the optimal values of coefficients must be chosen. In this study, the coefficients included in the design of the bacterial model were determined by previous experimental evidence and random search methods, as explained below.

4.1 Coefficient Settings Based on Experimental Evidence

Coefficients were determined depending on the experimental results [8] as follows:

$$\begin{aligned} C_{ap}(t) + C_a(t) &= 2.5\ \mu\text{M}, \\ C_{yp}(t) + C_y(t) &= 10.0\ \mu\text{M}, \\ C_{bp}(t) + C_b(t) &= 2.0\ \mu\text{M}. \end{aligned} \tag{22}$$

The direction of the flagellar rotation was determined using the time constant $T_s = 0.2$ s, and the swimming velocity was set at $v = 50$ μm/s. Additionally, in the tumbling state, the value of v was set at 0 μm/s. The angle θ between the conic central axis and the bus bar was set at 27 deg during swimming and 103 deg during tumbling.

4.2 Adjustment of the Coefficients Using a Genetic Algorithm

There are 12 invariable coefficients in the transducer component (v_{12}, v_{21}, v_{23}, v_{34}, v_{43}, $v_{12'}$, $v_{2'1}$, $v_{3'4'}$, $v_{4'3'}$, $v_{4'1}$, f_{41}, and $f_{2'3'}$) and 10 invariable coefficients in the intracellular signal transduction component

(v_b, v_y, v_{yz}, f_{bp}, f_a, f_{ap}, f'_a, f'_{ap}, f_{yp}, and k_{ap}). Because the CheZ concentration is fixed at $C_z(t) = 20$ μM, two coefficients can be combined into $v'_y = v_{yz}C_z(t) + v_y$. Therefore, the total number of invariable coefficients is $N = 21$. We adjusted these values adequately using a genetic algorithm (GA) [11, 23], which is a type of random search of the relevant solutions and is based on the evolution of actual organisms. The invariable coefficients were determined based on the concentrations of proteins expressed by the chemotaxis genes, which describe the characteristics of each protein. The optimal set of coefficients can be determined by simulating the evolution of the bacterial cell using a binary-coded GA [11]. First, all the invariable coefficients that are required to be well adjusted are included as the nth ($n = 1, 2, \ldots, N$) gene in a GA string X_p, where p is the serial number ($p = 1, 2, \ldots, P$) of the individual. The artificial genes for each population are expressed by $l \times N$ bits, where each coefficient is expressed by l bits of binary code. The movements of the virtual bacteria reflect uniform numbers for swimming directions that have been assigned randomly as described in Section 3.3. Therefore, in this study, m patterns of different initial positions of a virtual bacterium were considered. Additionally, the initial direction of bacterial movement was changed in the x-y plane, where the angle between the x axis and the direction vector of the bacterium was selected from among R different values (see Figure 4). Therefore, considering these conditions here, $Q = m \times R$. After making the above preparations, a GA [11] was employed, and the procedure used in this study is described below.

- *Step 0: Initialization.* N individuals of the initial generation were determined randomly with a uniform distribution. Moreover, the fitness function $F(X_p)$, which is the evaluation standard of the pth GA individual, is given by

$$F(X_p) = \frac{F_{\text{atr}}(X_p) + F_{\text{rpl}}(X_p)}{2}, \tag{23}$$

where $F_{\text{atr}}(X_p)$ and $F_{\text{rpl}}(X_p)$ are the fitness values for the attractants and repellents, respectively, and are calculated as follows:

$$F_{\text{atr}}(X_p) = \frac{1}{Q}\sum_{q=1}^{Q}\left(\frac{1}{t_f}\sum_{t=1}^{t_f}\frac{C_{\text{atr}}^{(p,q)}(t)}{C_{\text{atr}}^{(p,q)}(0)}\right), \tag{24}$$

$$F_{\text{rpl}}(X_p) = \frac{1}{Q}\sum_{q=1}^{Q}\left(\frac{1}{t_f}\sum_{t=1}^{t_f}\frac{C_{\text{rpl}}^{\max} - C_{\text{rpl}}^{(p,q)}(t)}{C_{\text{rpl}}^{\max} - C_{\text{rpl}}^{(p,q)}(0)}\right). \tag{25}$$

In these equations, $C_{\text{atr}}^{(p,q)}(t)$ and $C_{\text{rpl}}^{(p,q)}(t)$ are the concentrations of the attractants and repellents at time t for the pth individual in the qth condition; these values are calculated

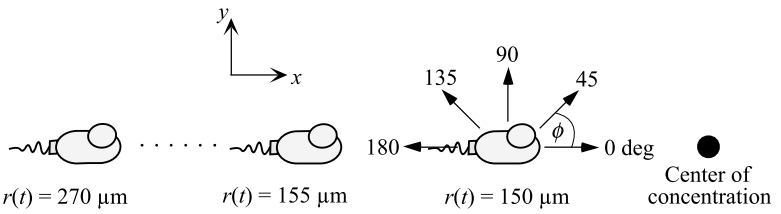

Figure 4. Initial positions and directions of movement of the virtual bacterium. In the computer simulations, 25 patterns of different initial positions of a virtual bacterium were considered, where the distance from the concentration center of chemicals on the x-y plane was increased by 5 μm in the sequence 150, 155,…, 270 μm. Additionally, the angle between the x axis and the direction vector of the bacterium was selected from five different values ($R = 5$): $\varphi = 0$, 45, 90, 135, and 180 deg.

using Equations 20 and 21, respectively. $C_{\mathrm{atr}}^{(p,q)}(0)$ and $C_{\mathrm{rpl}}^{(p,q)}(0)$ are the concentrations per unit time of $C_{\mathrm{atr}}(t)$ and $C_{\mathrm{rpl}}(t)$ that a bacterium can sense at the initial position. As an example, we consider chemical coenvironments using Equation 20 for attractants and Equation 21 for repellents. Under these settings, $F_{\mathrm{atr}}(X_p)$ increases as the bacterium moves toward the center of the environment defined by Equation 20, where the concentration of the attractants increases around the center. Furthermore, $F_{\mathrm{rpl}}(X_p)$ also increases as the bacterium moves toward the center in the environment defined by Equation 21, where the concentration of repellents decreases around the center. Virtual bacteria with fixed coefficients were evolved separately for the attractant and repellent concentrations for t_f. Based on the fitness value, the following three steps of (1) selection, (2) crossover, and (3) mutation were carried out in each generation $g = 1, 2, \ldots, G$.

- *Step 1: Selection.* An elite method [11] was employed for the selection of individuals in every generation. Each individual X_p was arranged in order, based on $F(X_p)$. Then, α individuals with a large fitness value were selected and saved in the next generation.
- *Step 2: Crossover.* To generate $P - \alpha$ new individuals, a uniform crossover method was adopted [11]. Two individuals were selected randomly as parents from P individuals in the current generation. Overlap was permitted in this selection. Each of the progeny genes of a new individual was selected from the two parents at identical probabilities. This crossover was repeated for each of the $P - \alpha$ individuals.
- *Step 3: Mutation.* The individuals for mutation were selected randomly, based on the mutation rate β. Each bit value included in the selected $\beta \times P$ individuals was inverted, that is, 1 turned to 0 and 0 turned to 1.
- *Step 4: Update.* The procedure from steps 1–3 was repeated for G.

4.3 Reproduction of Chemotaxis by Virtual Bacteria

We performed computer simulations of bacterial evolution using the proposed virtual bacteria. As described previously, the total number of coefficients was $N = 21$, where each coefficient was expressed by $l = 8$ bits. The number of generations was set at $G = 500$, and the number of individuals in a generation was $P = 16$; we set $\alpha = 2$ and $\beta = 1 \times 10^{-2}$. We set the environment of attractants using Equation 20, and that of repellents using Equation 21. In both equations defining the chemical concentrations, we set $r_{\mathrm{near}} = 20$ μm and $r_{\mathrm{far}} = 500$ μm. In this study, $m = 25$ patterns of different initial positions of a virtual bacterium were considered, where the distance from the concentration center of chemicals on the *x*-*y* plane increased in steps of 5 μm in the sequence 150, 155,…, 270 μm (see Figure 4). Additionally, the angle between the *x* axis and the direction vector of the bacterium

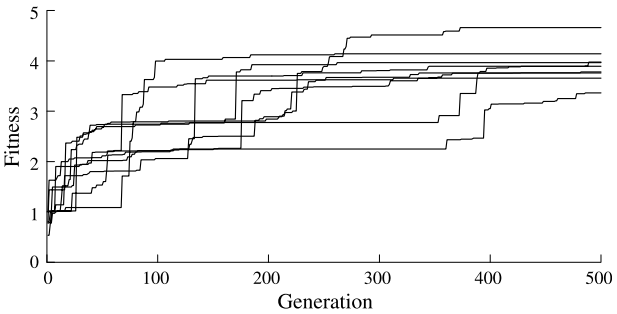

Figure 5. Evolution of the maximum fitness of the virtual bacteria. Nine trials were performed by changing the initial parameters, and the changes in maximum fitness were plotted until the 500th generation.

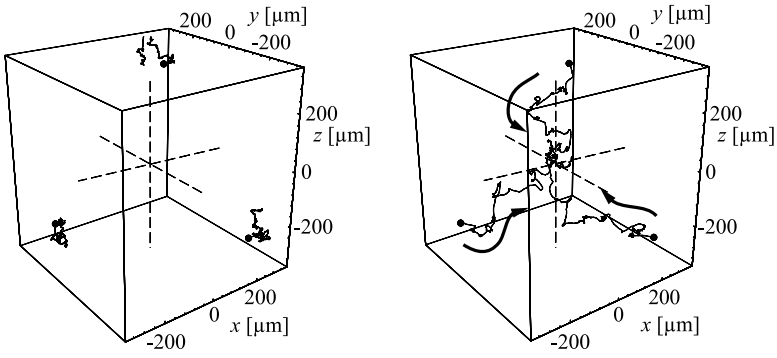

Figure 6. Trajectories of the virtual bacteria in response to attractants. (a) and (b) are the traces of the individuals in the 1st and 500th generations, respectively, where the filled circles denote the three types of initial positions. In the computer simulations, the concentrations of attractants were increased around the center of the environment, according to Equation 20.

was selected from five different values ($R = 5$): $\varphi = 0$, 45, 90, 135, and 180 deg (see Figure 4). Therefore, considering these conditions, $Q = 25 \times 5 = 125$. Simulations were carried out with $t_f = 100$ s. The ranges of the coefficients were determined by trial and error and were as follows: v_{12}, v_{34}, $v_{12'}$, $v_{3'4'}$, f_{41}, $f_{2'3'}$, $k_{ap} \in [0, 25.5]$; v_{21}, $v_{4'3'}$, $v_y \in [0, 12.75]$; v_{23}, $v_{4'1}$, $v_b \in [0, 1.275]$; v_{43}, $v_{2'1}$, f_a, f_a', $f_{yp} \in [0, 2.55]$; f_{ap}, $f_{ap}' \in [0, 51]$; and $f_{bp} \in [0, 0.85]$.

Figure 5 shows the changes in the maximum fitness value until the 500th generation, where nine trials were performed by changing the initial parameters. The maximum fitness increased as the generation progressed. Figures 6 and 7 show the trajectories of the virtual bacteria in response to the attractants and repellents, respectively. In these figures, (a) and (b) are the traces of the individuals in the 1st and 500th generations, respectively, where the filled circles denote the three types of initial positions. In the computer simulations, the concentrations of repellents as well as those of attractants were increased around the center of the environment, according to Equation 20.

From both Figures 6 and 7, it can be seen that the virtual bacteria barely moved from their initial positions in the 1st generation. In contrast, in the 500th generation they moved toward the concentration center of the attractants and escaped from the concentration center of the repellents. Thus, it was

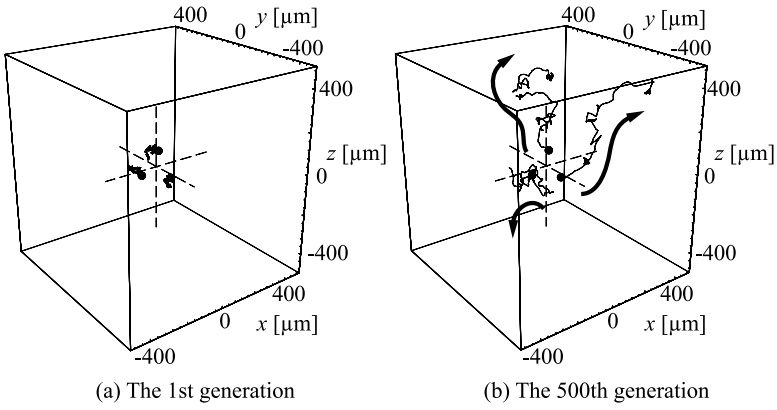

Figure 7. Trajectories of the virtual bacteria in response to repellents. (a) and (b) are the traces of the individuals in the 1st and 500th generations, respectively, where the filled circles denote the three types of initial positions. In the computer simulations, the concentrations of repellents as well as those of attractants were increased around the center of the environment, according to Equation 20.

verified that bacterial chemotaxis to attractants and repellents could be reproduced by the virtual bacteria using an evolved set of coefficients.

4.4 Analysis of Chemotaxis of Virtual Bacteria

We analyzed the chemotactic responses of the virtual bacteria from the following three viewpoints: (1) temporal behaviors, (2) chemotactic responses to chemical concentrations, and (3) chemotactic responses to multiple stimuli.

We first analyzed the accumulation of the virtual bacteria with respect to elapsed time. In this simulation, 300 virtual bacteria with identical coefficients were set randomly within an area on the x-y plane: $-300\ \mu m < x < 300\ \mu m$ and $-300\ \mu m < y < 300\ \mu m$. To investigate the time course of the chemotactic responses to attractants and repellents, virtual bacteria within the radii from the concentration center were counted every 5 s for 100 s. The responses of virtual bacteria to attractants and repellents (whose concentrations were determined again by Equations 20 and 21, respectively: that is, the attractant was mostly concentrated at the center, whereas the repellent was in the outer areas) are shown in Figure 8 as the time course of the distribution of 300 bacterial cells. It can be observed that the numbers of virtual bacteria moving toward the center increased with time and that this number became stable after a certain period, when the population within the area did not change drastically. This indicates that each virtual bacterium could show chemotactic responses to the attractants and repellents identical to those of an actual living bacterium.

We next investigated bacterial accumulation corresponding to the concentration of the attractants by comparing it with the actual responses. The chemotaxis of actual bacteria was measured experimentally using *E. coli* strain EJ500. The procedures of chemotaxis assay and computer analysis essentially followed a reported method [21], that is described in the Appendix. In this assay, to quantify the chemotactic behavior toward the attractant, bacterial accumulation was recorded using the phase-contrast microscope (magnification ×300) with the focus maintained at the mouth of the

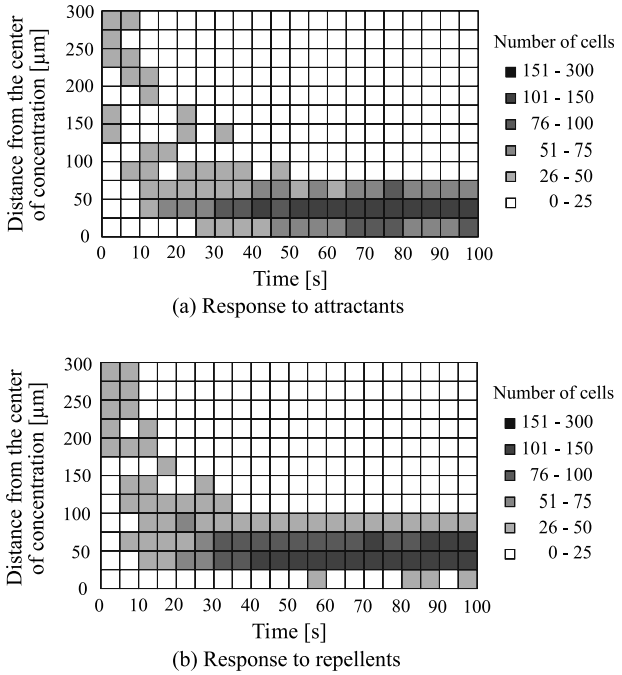

Figure 8. Time course of chemotactic responses of the virtual bacteria: (a) response to attractants; (b) response to repellents. The virtual bacteria within the radii from the concentration center were counted every 5 s for 100 s. There were 300 virtual bacteria in each simulation.

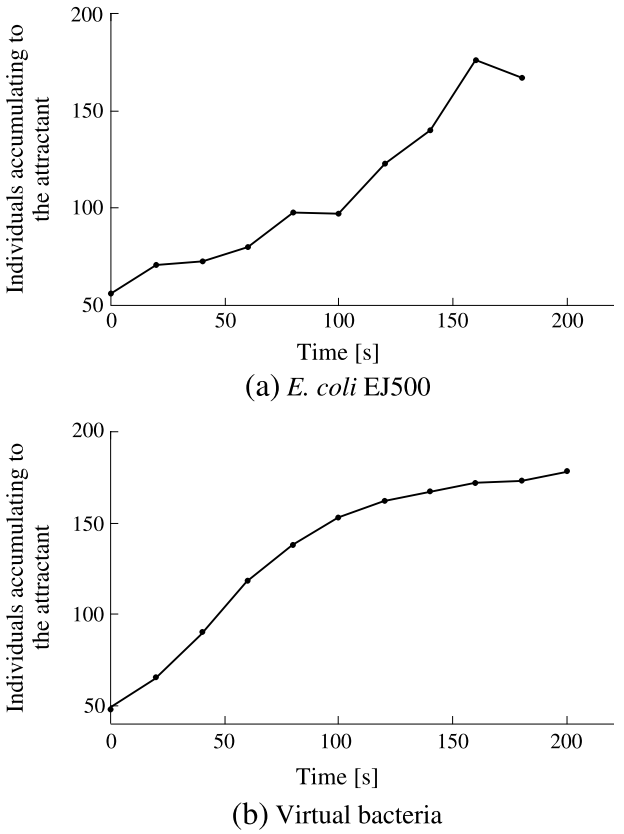

Figure 9. Chemotactic responses to attractants in the actual and virtual bacteria. (a) Response of the actual *E. coli* to 1×10^{-3} M of L-serine. (b) Response of the virtual bacteria to a concentration gradient of the attractant in which the maximum concentration was 20 μM.

capillary. On the other hand, computer simulations corresponding to the above experiments by using virtual bacteria were also carried out. We used a concentration gradient in which the maximum concentration at the center of the attractant was set at 20 μM. Initially, 200 virtual bacteria were placed at 2.5-μm intervals on the x axis at positions ranging from 0 (the center of the attractant) to 500 μm. The initial direction of motion was set randomly. After the predetermined duration, only virtual bacteria whose distance from the center of the attractant was within 120 μm were counted as individuals that had moved toward the center of the attractant. Figure 9a and b show the changes in the number of the actual and virtual bacteria that accumulated in the attractant locality as a function of time. In both results, increases of population around the attractant were observed with time, although there was a difference in the accumulation speed. Additionally, after a certain period the accumulated population tended to a steady state and did not change: This was common to both actual and virtual bacteria.

Bacterial accumulation around attractants was then investigated in more detail. As in the previous simulation shown in Figure 8, 300 virtual bacteria with identical coefficients were set randomly within an area on the x-y plane: $-300\ \mu m < x < 300\ \mu m$ and $-300\ \mu m < y < 300\ \mu m$. The number of bacterial cells within a radius of 100 μm from the concentration center was counted after 100 s. The maximum value at the concentration center of the attractants was changed, and simulation experiments were executed with 12 different chemical concentrations ranging from 0.02 to 120 μM, where the standard concentration was set at 20 μM. Figure 10 shows the change in bacterial accumulation corresponding to the change in the concentration of the attractants, where the mean value and the standard deviation of five trials have been plotted. From Figure 10, it can be seen that

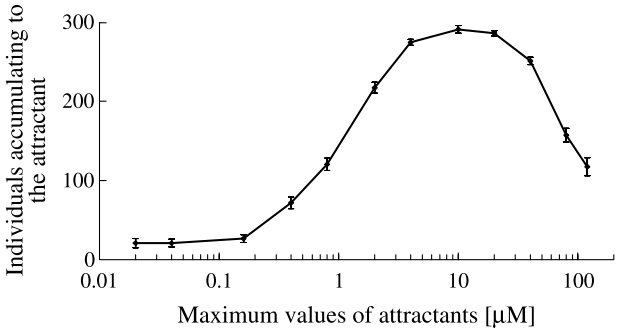

Figure 10. Concentration-dependent response of the virtual bacteria to attractants. The number of bacterial cells within a radius of 100 μm from the concentration center was counted after 100 s. The maximum value at the concentration center of the attractants was changed, and simulation experiments were executed with 12 different chemical concentrations ranging from 0.02 to 120 μM, where the standard concentration was set at 20 μM. The mean and standard deviation of five trials in each concentration setting are plotted.

the bacterial accumulation near the attractants increased with the attractant concentration and then gradually decreased after exceeding a peak value. Figure 11 shows the responses of the actual bacteria to a chemoattractant, namely L-serine. The number of bacterial cells was counted after 180 s. In this figure, the mean value and the standard deviation of five trials have been plotted. Comparing Figure 11 with Figure 10, it can be observed that the responses of actual and virtual bacteria were similar.

Finally, the chemotactic responses of virtual bacteria to multiple stimuli were examined in experiments involving both attractants and repellents. The chemical concentrations of attractants and repellents in the environments were both determined by Equation 20, where $r_{near} = 20$ μm and $r_{far} = 500$ μm for the attractants and $r_{near} = 20$ μm and $r_{far} = 300$ μm for the repellents. Thus, both the attractants and repellents were included within a circle with a radius of 300 μm, whereas only the attractants were included between the two circles with radii 300 and 500 μm. In this chemical environment, 300 individuals with identical coefficients were set randomly in an area on the x-y plane: -300 μm $< x <$ 300 μm and -300 μm $< y <$ 300 μm. Because the swimming velocity was 50 μm/s, it would take at least 6 s to swim 300 μm even if any change in the swimming direction were neglected. The bacterial responses were then observed by plotting the position of each individual at time $t = 0$, 10, 50, and 100 s. From Figure 12, it can be observed that the virtual bacteria approached the boundary between the attractants and repellents. These results indicate that the bacterial response could be controlled roughly by the chemical stimuli in the environment.

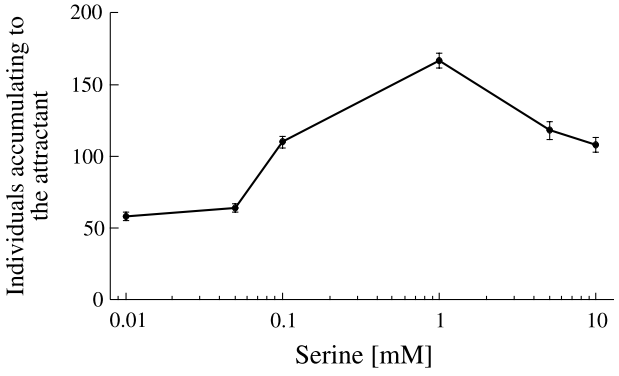

Figure 11. Concentration-dependent response of the actual *E. coli* to the attractant, L-serine. The number of bacterial cells was counted after 180 s, and the mean and standard deviation of five trials are plotted.

5 Mobile Robot Control Based on Bacterial Chemotaxis

Since the effectiveness and validity of the virtual bacterium were confirmed using a series of computer simulations, we applied it here to a mobile robot control problem. If a mobile robot using the bacterial algorithm (virtual bacteria) modeling the bacterial chemotactic response shows chemotactic behavior similar to that observed in actual bacteria, this indicates that the biomimetic control of artificial machines has been achieved.

As the first step of biomimetic control, we utilized a mobile robot that could run in the horizontal plane. Therefore, it was necessary to reduce the swimming movement (three-dimensional) to a running movement (two-dimensional) of the robot, although the intracellular information processing was the same as that in the simulation. Because the motor control model used in the computer simulation could not be directly applied to robot control, we partially modified the model prior to use. In the robot control experiments, we presented the stimulation condition by the color pattern of the floor instead of chemical materials. The robots sensed this external stimulation and its concentration as an

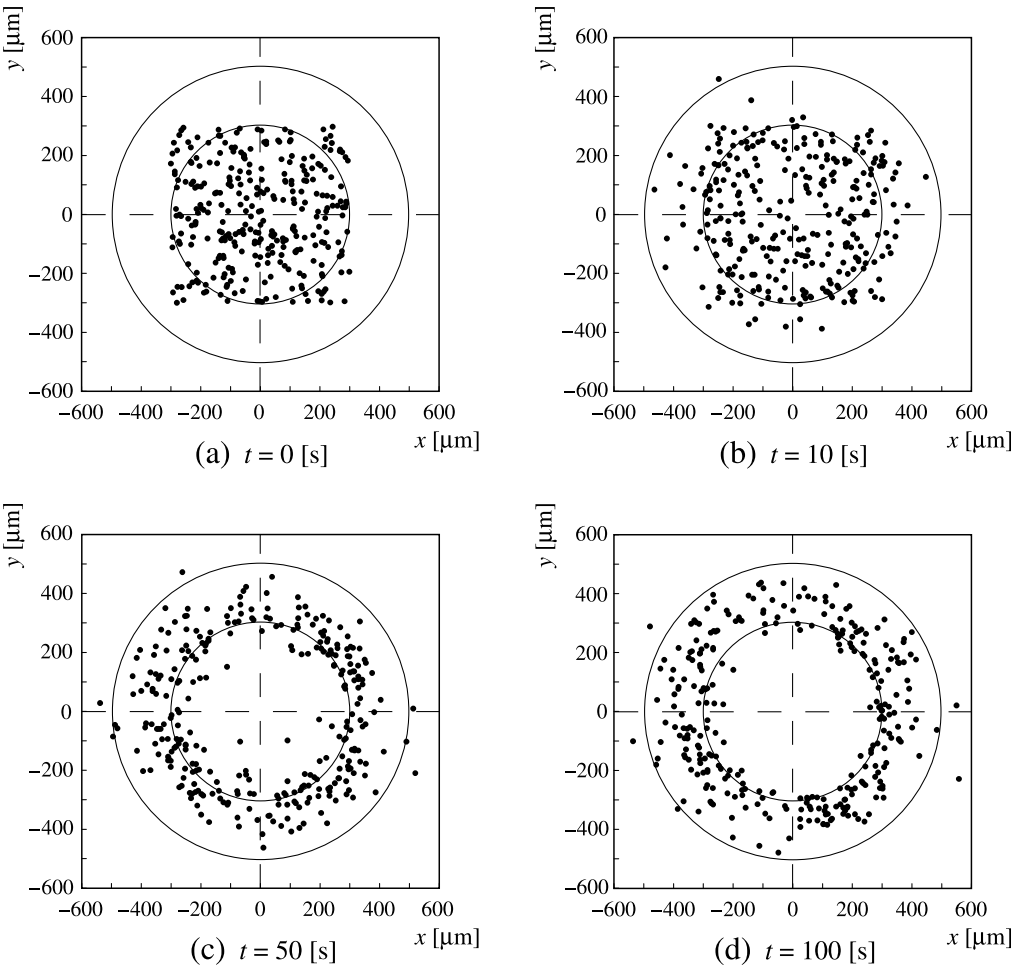

Figure 12. Time course of chemotactic responses of the virtual bacteria to attractants and repellents. In this experiment, 300 individuals with identical coefficients were set randomly in an area on the *x*-*y* plane: $-300\ \mu m < x < 300\ \mu m$ and $-300\ \mu m < y < 300\ \mu m$. The position of each individual is shown at four time points: (a) $t = 0$ s, (b) $t = 10$ s, (c) $t = 50$ s, and (d) $t = 100$ s. The chemical concentrations of attractants and repellents in the environments were both determined by Equation 20, where $r_{near} = 20\ \mu m$ and $r_{far} = 500\ \mu m$ for the attractants, and $r_{near} = 20\ \mu m$ and $r_{far} = 300\ \mu m$ for the repellents.

optical stimulation and processed the information according to the intracellular model for chemotactic response.

5.1 Structure of the Mobile Robot

In these experiments, we used the Rug Warrior Pro Mobile Robot Kit (A. K. Peters, Ltd., Natick, MA, USA) for the robot. The Rug Warrior has a circular body approximately 160 mm in diameter and is equipped with two 6-V gear motors that drive two wheels (approximately 60 mm in diameter) independently, a MC68HC11A1 microcontroller (Motorola Ltd., Schaumberg, IL, USA) as a CPU, and a photosensor for environmental searching (see Figure 13a). Programs for Rug Warrior are written in the programming language Interactive C, and the code is downloaded to the robot via a serial port. The robot could calculate intracellular signal processing, but the processing speed of the CPU decreased when this was done. Therefore, all signal-processing calculations were performed on a desktop computer and transmitted to the robot at a sampling frequency of 1 kHz.

The mobile robot moved on a board with an area of 1.82 m × 1.82 m; a shading pattern was drawn on this board to represent the gradient of the attractant or repellent concentration (see Figure 13b) instead of Equations 20 and 21 in the previous computer simulation. The shaded pattern consisted of concentric circles with a 13-step gradation at 0.07-m intervals, where the smallest circle had a radius of 0.07 m; the shading became darker toward the center of the pattern. The robot searched for the location where the degree of shading was the lowest in its operational space. Thus, the robot measured the degree of shading on the floor surface using a photosensor and converted this into a virtual chemical concentration. The concentration set virtually on the board, ${}^{\mathrm{robo}}C_{\mathrm{chem}}(r)$, was calculated using the following equation:

$$ {}^{\mathrm{robo}}C_{\mathrm{chem}}(r) = C_{\mathrm{chem}}^{\max}\left(\frac{S(r) - S^{\min}}{S^{\max} - S^{\min}}\right), \tag{26} $$

where $C_{\mathrm{chem}}^{\max}$ (chem $\in$ {atr, rpl}) is the maximum concentration of the attractant or repellent. $S(r)$ denotes the value of the photosensor at the current distance $r(t)$ from the center of the chemical concentration; $S^{\max}$, the value at the center of the board; and $S^{\min}$, the lowest value on the board. In these

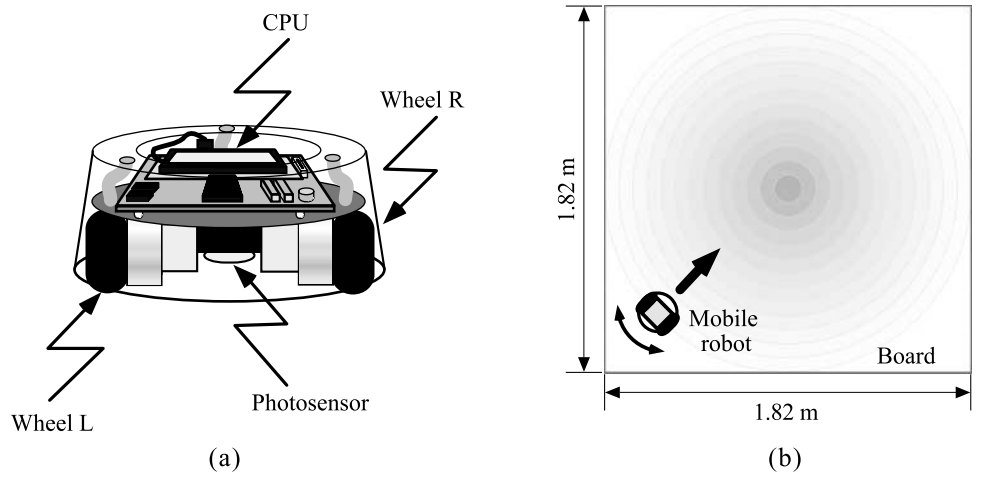

Figure 13. Mobile robot and its experimental environment. (a) The robot was equipped with a CPU chip (MC68HC11A1, Motorola Ltd.) and a photosensor. It could calculate virtual intracellular signal processing after an operational program had been installed. (b) Overhead view of an experiment field for mobile robot control. The robot moved on a board with an area of 1.82 m × 1.82 m; a shading pattern was drawn on this board to represent the gradient of the attractant or repellent concentration. The shaded pattern consisted of concentric circles with a 13-step gradation at 0.07-m intervals, where the smallest circle had a radius of 0.07 m; the shading became darker toward the center of the pattern.

experiments, we considered an environment with attractant and set $C_{\mathrm{atr}}^{\max}$ at 20 μM. Using Equation 26, we could deal with a concentric circle with a 13-step gradation on the board, as with the chemical concentration. In this environment, the autonomous mobility of the robot was examined using the model of chemotaxis in *E. coli*.

5.2 Model of the Mobile Robot

Figure 14 shows the model of the mobile robot used in the experiments. Σ_w was the world coordinate system fixed in the environment, and Σ_c was the moving coordinate system whose origin was set at the midpoint between the two wheels of the robot, with its x axis oriented along the direction of the motion. Thus, the following generalized coordinates of the robot could be selected: the position (x, y) and orientation angle ${}^{\mathrm{robo}}\theta$ of Σ_c with respect to Σ_w.

The angular velocities of the right and left wheels were denoted as v_R, v_L, respectively, and the translational velocity in the x direction and the rotational velocity of the mobile robot were denoted as v and ω, respectively. The relationship between the driving velocity vector $\boldsymbol{u} = (v, \omega)^{\mathrm{T}}$ and the wheel velocity vector $\boldsymbol{s} = (v_R, v_L)^{\mathrm{T}}$ was obtained by the following equations:

$$\boldsymbol{u} = \boldsymbol{K}\boldsymbol{s}, \tag{27}$$

$$\boldsymbol{K} = -L\begin{bmatrix} \frac{1}{2} & \frac{1}{2} \\ \frac{2}{W} & -\frac{2}{W} \end{bmatrix}, \tag{28}$$

where L is the radius of the wheels and W is the distance between the right and left wheels (see Figure 14). Since the relationship between $\boldsymbol{s}$ and $\boldsymbol{u}$ is always a one-to-one correspondence, $\boldsymbol{u}$ was selected as the system input. Therefore, the mobile robot was controlled by the angular velocities of the right and left wheels, that is, v_R, v_L.

The mobile robot could exhibit only two types of behavior: swimming (translational movement) and tumbling (turning movement). In the swimming behavior, the robot moved straight in the current direction ${}^{\mathrm{robo}}\theta$ with a translational velocity of 0.2076 m/s for 0.5 s ($\omega = 0$). Alternatively, in the tumbling

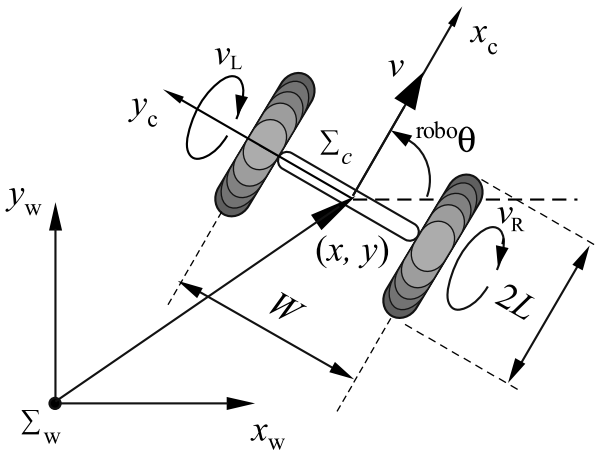

Figure 14. Motor control model of the mobile robot with two wheels. Σ_w is the world coordinate system fixed in the environment, and Σ_c is the moving coordinate system whose origin was set at the midpoint between the two wheels of the robot, with its x axis oriented along the direction of the motion. L is the radius of the wheels, and W is the distance between them. The generalized coordinates of the mobile robot can be selected as the position (x, y) and orientation angle ${}^{\mathrm{robo}}\theta$ of Σ_c with respect to Σ_w. The angular velocities of the right and left wheels are denoted as v_R, v_L, respectively.

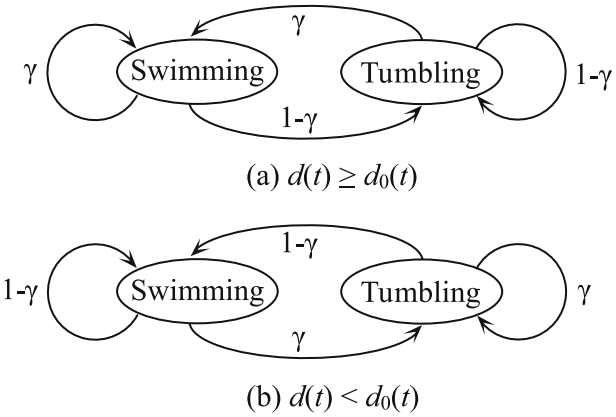

Figure 15. State transition model of the flagellar motor. This corresponds with assigning the swimming direction uniform numbers randomly in the computer simulation. In this model, we defined $0.5 > \gamma \geq 1.0$. Under these settings, (a) the robot typically tended to exhibit swimming behavior when $d(t) \geq d_0(t)$; (b) the robot exhibited tumbling behavior when $d(t) < d_0(t)$.

behavior, the robot selected the next swimming direction randomly and turned toward the selected direction for 1 s ($v = 0$). Considering the computational load, the direction was selected from only 10 different directions that were determined by dividing 360 deg equally. To change the attractant concentration, swimming was performed compulsorily after every tumbling behavior. Furthermore, to reproduce the behaviors of the actual bacteria, which are influenced by random noises in the environment, the rotational direction of the flagellar motor was determined according to a state transition model, as shown in Figure 15. This corresponds with assigning the swimming direction uniform numbers randomly in the computer simulation. In this model, we set $0.5 > \gamma \geq 1.0$. Under this setting, the mobile robot typically tended to exhibit swimming behavior when $d(t) \geq d_0(t)$ (see Figure 15a), whereas it exhibited tumbling behavior when $d(t) < d_0(t)$ (see Figure 15b). In this way, the probability of exhibiting the tumbling state was reduced with a decrease in the state-transition probability γ.

5.3 Regulation of Coefficients for the Mobile Robot

We regulated the coefficients for the mobile robot using the same GA method described in Section 4.2. However, because more time was required to regulate the coefficients of intracellular signal processing while controlling the real robot, the experiment with the robot was conducted using the evolved coefficients employed in the computer simulations and physical conditions that were almost identical to the actual environment. The coefficients included in the velocity of the robot and the degrees of shading in the pattern were measured using a photosensor attached to the robot.

At first, we set the virtual chemical concentrations (μM) of proteins, C_a, C_{ap}, C_b, C_{bp}, C_y, and C_{yp}, at random numbers that satisfied Equation 22. In this experiment, to reduce the calculation load on the CPU, the processing system for the repellents was excluded ($v_{12'} = v_{2'1} = v_{3'4'} = v_{4'3'} = v_{4'1} = f_{2'3'} = f'_{ap} = f'_a = 0$). Consequently, the total number of coefficients in the computer model was $N = 13$. The evolution for $t_f = 120$ s was executed for each individual with $l = 8$ bits, $G = 200$, $P = 16$, and a repetition number $Q = 125$ by changing the initial values using random numbers with a uniform distribution. The range for each coefficient was determined experimentally from preliminary experiments as follows: v_{12}, v_{34}, v'_y, f_{41}, $k_{ap} \in [5.9, 14.1]$; v_{23}, v_b, f_{bp}, $f_{yp} \in [0, 2.05]$; v_{43}, $f_a \in [0, 13.05]$; $v_{21} \in [1.9, 10.1]$; and $f_{ap} \in [15.9, 24.01]$. The initial values of each coefficient were set randomly within the search range, and γ was set to 0.5, 0.6, 0.7, 0.8, 0.9, and 1.0. The maximum fitness after evolution (in the 200th generation of the GA) improved with an increase in γ, whereas the standard deviations of multiple trials increased (Figure 16).

In the next subsection, we examine the movements of mobile robots using these coefficients and evaluate the effects of the GA-based coefficient regulation and γ value.

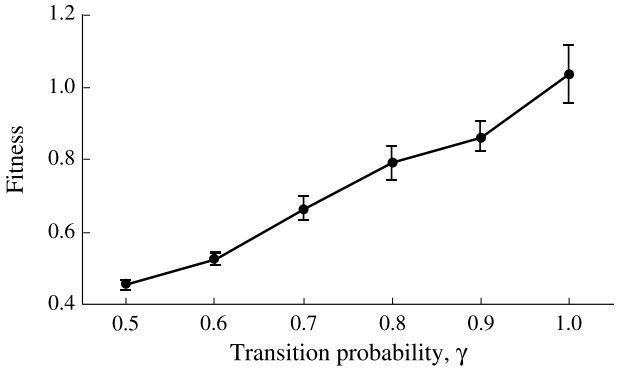

Figure 16. The γ dependence of the maximum fitness of the GA in the 200th generation for regulation of the coefficient setting for mobile robot control. The mean and standard deviation of 10 trials at each value of the state transition probability γ are shown. In coefficient regulation using the GA, the initial values of each coefficient were set randomly within the search range, and γ was increased from 0.5 to 1.0.

5.4 Experimental Results

We examined the mobile robot control using coefficients regulated by the GA. At first, to confirm the effect of GA-based coefficient regulation, we used both evolved and non-evolved sets of coefficients. Figure 17a and b show the trajectories of the robot using coefficients in the 1st and 200th generations, where $\gamma = 0.8$. These trajectories were measured for 30 s using a stereo camera system (QuickMag, OKK Inc., Tokyo, Japan) hanging from the ceiling. In these experiments, the concentration of attractants increased around the center of the environment. S1 and S2 denote the initial positions of the robot in different trials. Each point on the trajectories represents the position of the robot at 1 s. Comparing Figure 17a and b, we see that the robot using an evolved set of coefficients followed the concentration, that is, it could reproduce bacterial chemotaxis well, whereas the robot using a non-evolved set of coefficients could not. This indicates the importance of appropriate settings of coefficients.

Subsequently, to evaluate the influence of the γ value on the mobile robots movements, we used three sets of evolved coefficients obtained under different values of γ. Figure 18a, b, and c show the trajectories of the mobile robot using coefficients obtained under $\gamma = 0.6$, $\gamma = 0.8$, and $\gamma = 1.0$, respectively. These results indicate that the tendency of the robot to approach the center of attractant concentration became stronger with an increase in γ. This tendency well reflected the increase

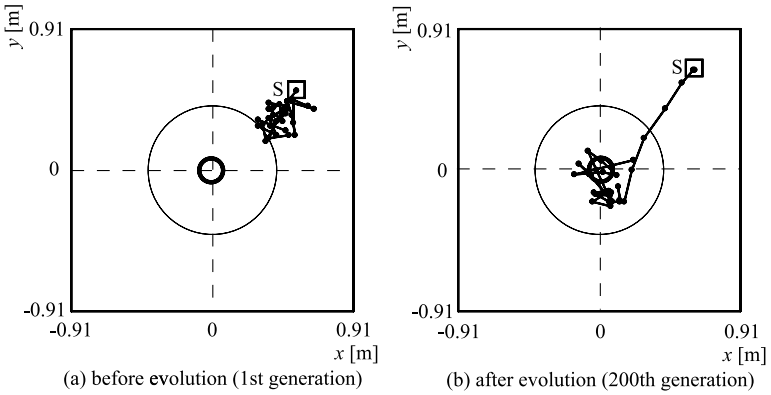

Figure 17. Comparison of mobile robot trajectories in relation to attractants, considering the evolution of coefficients. The trajectories were measured for 30 s using a stereo camera system (QuickMag, OKK Inc.) hanging from the ceiling, and S denotes the initial position of each robot. Each point on the trajectories represents the position of the robot at 1 s. The coefficients in (a) were in the 1st generation of GA, while those in (b) were in the 200th generation, where $\gamma = 0.8$.

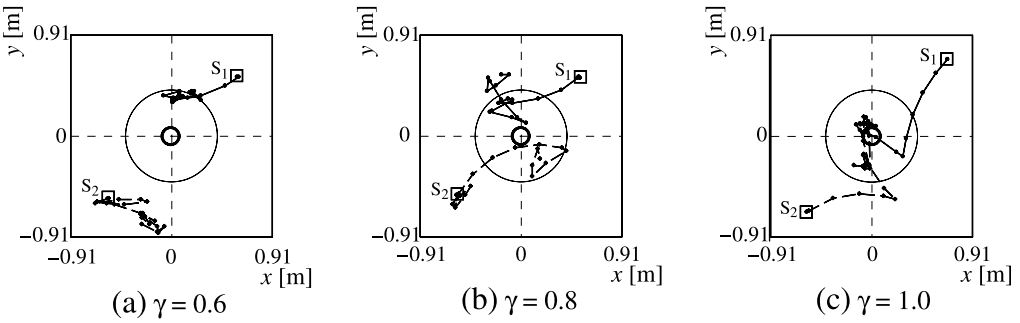

Figure 18. Comparison of mobile robot trajectories to attractants for various γ values. The trajectories were measured for 20 s using a stereo camera system as in Figure 17. The solid lines denote the trajectories of the robot started at S1, and the dashed lines denote those of the robot started at S2. Each point on the trajectories represents the position of the robot at 1 s. The γ values used in experiments were (a) $\gamma = 0.6$, (b) $\gamma = 0.8$, and (c) $\gamma = 1.0$. In all experiments, we used coefficients obtained in the 200th generation of the GA.

of fitness values in the GA described in the previous subsection (see Figure 16). Therefore, we can state that the bacterial chemotaxis model functioned to some extent in the actual environment, regardless of the existence of unknown noises.

Finally, we examined the movements of the robot from various initial positions and postures. The initial positions of the robot were set on the circumference of circles with five different radii starting from 0.42 m at 0.07-m intervals, and the initial postures were set in eight directions from 0 deg at 45-deg intervals. Thus, we conducted $5 \times 8 = 40$ trials; γ was set at 0.8, and the same set of coefficients evolved for 200 generations using a GA was used in each trial. A set of coefficient values obtained after the 200th GA generation under $\gamma = 0.8$ and used in Figures 17b and 18b, is shown in Table 1. The numbers of trials that were conducted using the robot within a circle of radius 0.42 m (the center region of chemical concentration) were counted every 5 s. The results of the 40 trials can be considered as the results for 40 distinct robots. Figure 19 shows these results. The figure confirms that the robot could reach the attractant area eventually, regardless of the initial position and posture, using an evolved set of coefficients. In this setting ($\gamma = 0.8$), the number of robots within the attractant area

Table 1. A set of 13 coefficient values included in the bacterial intracellular model for mobile robot control. These values were obtained after the 200th genetic algorithm generation under $\gamma = 0.8$ and used in Figures 17b and 18b. To reduce the calculation load on the CPU, the coefficients for the repellents, $v_{12'}$, $v_{2'1}$, $v_{3'4'}$, $v_{4'3'}$, $v_{4'1}$, $f_{2'3'}$, f'_{ap}, and f'_a, were set to 0.

Transducer components		Intracellular signal transduction components	
Symbol	Value	Symbol	Value
v_{12}	11.40	v_b	0.25
v_{21}	11.10	v'_y	8.75
v_{23}	0.60	f_{bp}	0.17
v_{34}	15.80	f_a	5.55
v_{43}	4.00	f_{ap}	27.20
f_{41}	2.20	f_{yp}	0.51
		k_{ap}	22.10

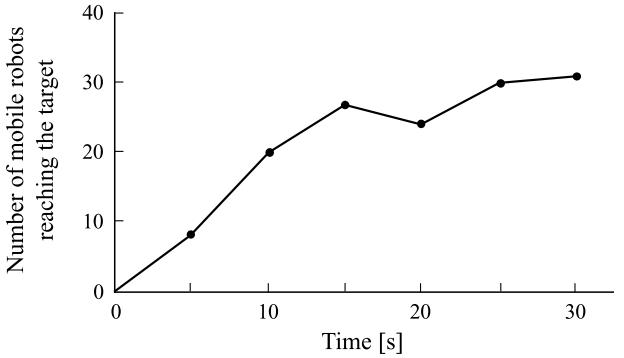

Figure 19. Chemotactic responses of the mobile robots. The initial positions of the robots were set on the circumferences of circles with five different radii starting from 0.42 m at 0.07-m intervals, and the initial postures were set in eight directions from 0 deg at 45-deg intervals. Thus, we conducted 40 trials; γ was set at 0.8, and the same set of coefficients evolved for 200 generations by using a GA was used in each trial. The number of trials that were conducted using the robot within a circle of radius 0.42 m (the center region of chemical concentration) was counted at every 5 s. The results of 40 trials can be considered as the results of 40 distinct robots.

was not 40. Once robots reached the center of attractant, they moved from place to place as shown in Figure 18b. As a result, some robots were observed in the area without attractants. This *swarming* behavior might be similar to that of actual bacteria.

6 Conclusion

The ultimate goal of our research is to develop "real" artificial machines that are able to respond adequately to a diverse range of situations, displaying complex or autonomous behaviors. We work under the hypothesis that this goal is achievable if the environmental recognition mechanisms occurring naturally in living organisms (or even simplified versions of them) can be implemented in those machines. We established the following steps to realize the biomimetic control of artificial machines: (1) modeling the responses to environments in living organisms and evaluating the computer model through a series of simulations, and (2) evaluating the validity of the computer model of living organisms as a motor-control algorithm through motor-control experiments of artificial machines using the model.

In this article, we have focused on the chemotactic response of *E. coli* and have constructed a computer model known as *virtual bacteria*, based on molecular evidence. Two main results were obtained using our computer simulations. First, we proved that the virtual bacteria could reproduce chemotactic responses to attractants and repellents. Second, we showed that chemical conditions had a clear influence on the behavior of these virtual bacteria. A sort of adaptive behavior to their environment in the course of time was also realized.

Then, we applied the model of the bacterial intracellular signal processing to control mobile robots. In doing so, we verified experimentally that such robots can indeed realize "living" behaviors such as bacterial chemotaxis. The control system of the robots is implemented in software and executed using a microprocessor, while a bacterial system is a wet computing system. However, our results on robot control suggest that the two systems are essentially equivalent to each other and that biological information processing can be applicable to the control problems of artificial machines. In particular, the possibility of robot control based on the phosphorylation-dephosphorylation reaction of protein was confirmed. This means that even microrobot control is achievable using chemical chips based on protein reactions. From this point of view, our success in biomimetic control is only an example, but represents a major step in studies on artificial life.

Information processing by living organisms involves greatly diverse aspects. In parallel with the bacterial model, we have developed models of two other organisms [16, 17, 28, 29]. One is the paramecium [32], a unicellular organism that processes stimulation information by electrical signals, and the other

is the nematode *Caenorhabditis elegans* [30, 31], which has both neuronal circuits for information processing and muscles for complicated movements. Thus, we aim to arrange several types of information-processing algorithms of living organisms systematically, from a protozoan to a multicellular organism, and enable artificial machines to adopt the most suitable method, among various algorithms, depending on the specific problems they face or are designed to face.

Acknowledgments

The authors thank Dr. Tomohiro Morohoshi for his contribution during the early years of modeling, and Dr. Makoto Kaneko for his valuable advice on mobile robot control. We also thank Dr. Yoshiyuki Tanaka, Dr. Osamu Fukuda, Mitsuru Murakami, Koji Hashigami, Dr. Akira Sakane, and Dr. Akira Hirano for their kind assistance in experiments on mobile robot control. M.S. was supported by a research fellowship of the Japan Society for the Promotion of Science (JSPS) for JSPS Fellows.

References

1. Barkai, N., & Leibler, S. (1997). Robustness in simple biochemical networks. *Nature*, *387*(6636), 913–917.
2. Berg, H. C. (1983). *Random walks in biology*. Princeton, NJ: Princeton University Press.
3. Berg, H. C., Block, S. M., Conley, M. P., Nathan, A. R., Power, J. N., & Wolfe, A. J. (1987). Computerized video analysis of tethered bacteria. *Review of Scientific Instruments*, *58*(3), 418–423.
4. Bourret, R. B., Borkovich, K. A., & Simon, M. I. (1991). Signal transduction pathways involving protein phosphorylation in prokaryotes. *Annual Reviews of Biochemistry*, *60*(1), 401–441.
5. Boyd, A., & Simon, M. (1982). Bacterial chemotaxis. *Annual Reviews of Physiology*, *44*(1), 501–517.
6. Bray, D. (1995). Protein molecules as computational elements in living cells. *Nature*, *376*, 307–312.
7. Bray, D. (2002). Bacterial chemotaxis and the question of gain. *Proceedings of the National Academy of Sciences of the United States of America*, *99*(1), 7–9.
8. Bray, D., & Bourret, R. B. (1995). Computer analysis of the binding reactions leading to a transmembrane receptor-linked multiprotein complex involved in bacterial chemotaxis. *Molecular Biology of the Cell*, *6*(10), 1367–1380.
9. Bray, D., Bourret, R. B., & Simon, M. I. (1993). Computer simulation of the phosphorylation cascade controlling bacterial chemotaxis. *Molecular Biology of the Cell*, *4*(5), 469–482.
10. Bray, D., & Lay, S. (1994). Computer simulated evolution of a network of cell-signaling molecules. *Biophysical Journal*, *66*(4), 972–977.
11. Goldberg, D. E. (1989). *Genetic algorithms in search, optimization and machine learning*. Reading, MA: Addison-Wesley Longman Publishing.
12. Hauri, D. C., & Ross, J. (1995). A model of excitation and adaptation in bacterial chemotaxis. *Biophysical Journal*, *68*(2), 708–722.
13. Hazelbauer, G. L. (1988). The bacterial chemosensory system. *Canadian Journal of Microbiology*, *34*(4), 466–474.
14. Hazelbauer, G. L. (2005). Myriad molecules in motion: Simulated diffusion as a new tool to study molecular movement and interaction in a living cell. *Journal of Bacteriology*, *187*(1), 23–25.
15. Hazelbauer, G. L., Yaghmai, R., Burrows, G. G., Baumgartner, J. W., Dutton, D. P., & Morgan, D. G. (1990). Transducers: Transmembrane receptor proteins involved in bacterial chemotaxis. In *Proceedings of the 46th Symposium of the Society for General Microbiology jointly organized with the British Society for Cell Biology* (pp. 108–119).
16. Hirano, A., Tsuji, T., Takiguchi, N., & Ohtake, H. (2006). An electrophysiological model of chemotactic response in *Paramecium*. In *Proceedings of the 2006 IEEE International Conference on Systems, Man, and Cybernetics* (pp. 3612–3617).
17. Hirano, A., Tsuji, T., Takiguchi, N., & Ohtake, H. (2006). Biomimetic control of mobile robots based on the information processing model of *Paramecium*. In *Proceedings of the Eleventh International Symposium on Artificial Life and Robotics* (pp. 313–318).

18. Kato, J., Ito, A., Nikata, T., & Ohtake, H. (1992). Phosphate taxis in *Pseudomonas aeruginosa*. *Journal of Bacteriology*, *174*(15), 5149–5151.

19. Knox, B. E., Devreotes, P. N., Goldbeter, A., & Segel, L. A. (1986). A molecular mechanism for sensory adaptation based on ligand-induced receptor modification. *Proceedings of the National Academy of Sciences of the United States of America*, *83*(8), 2345–2349.

20. Macnab, R. M. (1997). Motility and chemotaxis. In F. C. Neidhardt (Ed.), *Escherichia coli and salmonella typhimurium*, Vol. 1 (pp. 732–759). Washington, DC: American Society for Microbiology.

21. Nikata, T., Sumida, K., Kato, J., & Ohtake, H. (1992). Rapid method for analyzing bacterial behavioral responses to chemical stimuli. *Applied Environmental Microbiology*, *58*(7), 2250–2254.

22. Oda, K., & Kitano, H. (2006). A comprehensive map of the toll-like receptor signaling network. *Molecular Systems Biology*, *2*, 2006.0015.

23. Pham, D. T., & Karaboga, D. (2000). *Intelligent optimization techniques*. London: Springer.

24. Stewart, R. C., & Dahlquist, F. W. (1987). Molecular components of bacterial chemotaxis. *Chemical Reviews*, *87*(5), 997–1025.

25. Stock, A. M. (1999). A nonlinear stimulus-response relation in bacterial chemotaxis. *Proceedings of the National Academy of Sciences of the United States of America*, *96*(20), 10945–10947.

26. Stock, J. B., Ninfa, A. J., & Stock, A. M. (1989). Protein phosphorylation and regulation of adaptive responses in bacteria. *Microbiology and Molecular Biology Reviews*, *53*(4), 450–490.

27. Sugimoto, M., Takahashi, K., Kitayama, T., Ito, D., & Tomita, M. (2005). Distributed cell biology simulations with E-Cell system. In A. Konagaya & K. Satou (Eds.), *Lecture Notes in Computer Science, LNBI 3370* (pp. 20–31). Berlin: Springer.

28. Suzuki, M., Goto, T., Tsuji, T., & Ohtake, H. (2005). A dynamic body model of the nematode *C. elegans* with neural oscillators. *Journal of Robotics and Mechatronics*, *17*(3), 318–326.

29. Suzuki, M., Tsuji, T., & Ohtake, H. (2005). A model of motor control of the nematode *C. elegans* with neuronal circuits. *Artificial Intelligence in Medicine*, *35*(1–2), 75–86.

30. Tajima, T., Takiguchi, N., Kato, J., Ikeda, T., Kuroda, A., & Ohtake, H. (2003). Mutants of the nematode *Caenorhabditis elegans* that are defective specifically in their attraction to cycloheximide. *Journal of Bioscience and Bioengineering*, *96*(2), 149–153.

31. Tajima, T., Watanabe, N., Kogawa, Y., Takiguchi, N., Kato, J., Ikeda, T., Kuroda, A., & Ohtake, H. (2001). Chemotaxis of the nematode *Caenorhabditis elegans* toward cyclohexamide and quinine hydrochloride. *Journal of Bioscience and Bioengineering*, *91*(3), 322–324.

32. Takiguchi, N., Tajima, T., Asayama, K., Ikeda, T., Kuroda, A., Kato, J., & Ohtake, H. (2002). Behavioral responses of the ciliated protozoan *Paramecium caudatum* to 2,4-dichlorophenoxyacetic acid and its analogues. *Journal of Bioscience and Bioengineering*, *93*(4), 416–420.

33. Tomita, M., Hashimoto, K., Takahashi, K., Matsuzaki, Y., Matsushima, R., Saito, K., Yugi, K., Miyoshi, F., Nakano, H., Tanida, S., Saito, Y., Kawase, A., Watanabe, N., Shimizu, T. S., & Nakayama, Y. (2000). The E-CELL project: Towards integrative simulation of cellular processes. *New Generation Computing*, *18*(1), 1–12.

34. Tomita, M., Hashimoto, K., Takahashi, K., Shimizu, T. S., Matsuzaki, Y., Miyoshi, F., Saito, K., Tanida, S., Yugi, K., Venter, J. C., & Hutchison, C. A., 3rd. (1999). E-CELL: Software environment for whole-cell simulation. *Bioinformatics*, *15*(1), 72–84.

Appendix: Chemotaxis Assay and Computer Analysis

The procedures used in this study were described previously [21]. Bacteria were grown overnight in nutrient broth (Difco) in a 25-mL tubes at 37°C with shaking (100 to 250 rpm), inoculated into fresh medium (a 1% inoculum), and then incubated to the exponential phase of growth. Bacterial cells were harvested by centrifugation in a 2-mL Eppendorf tube for 1 min at 8,000*g* at room temperature, and the pellet was gently resuspended in 1 mL of chemotaxis medium (10 mM potassium phosphate buffer (pH 7.0) and 0.1 mM potassium EDTA). Bacterial cells were centrifuged and resuspended in chemotaxis medium to a concentration of ca. 6×10^8 cells/mL [21]. For microscopic observation of bacterial

motility, a small chamber was formed by laying a U-shaped glass tube (0.5 mm in diameter) as a spacer between two cover-slips and mounted on the stage of an IMT-2 inverted dark-field microscope (Olympus Co., Tokyo, Japan). Glass capillary tubes with internal diameters of 10–40 μm were prepared from micro-injection glass tubing using a microcapillary puller. Attracting agar was made by adding 1.5% agar to a chemotaxis medium containing an attractant such as L-serine and kept molten at 60°C. The glass capillary was plunged into a test tube containing attractant agar. The preferred length of the column of attractant agar in the capillary was about 10 ± 3 mm. Neither end of the capillary was sealed. After the exterior of the capillary had been rinsed quickly with distilled water, it was inserted carefully into the chamber on the stage of the IMT-2 microscope and moved to a particular position in the field of a microscopic view using a joystick micromanipulator (MN-151, Narishige Co., Tokyo, Japan). Bacterial cells in a 20-μL suspension were placed on a cover-slip. The cover-slip was immediately placed upside down on the U-shaped spacer to fill the chamber with the suspension. To quantify any chemotactic behavior toward the attractant, bacterial accumulation was video-recorded through a phase-contrast microscope (magnification ×300) with the focus maintained at the mouth of the capillary. A distance of 40 pixels in the video image was equivalent to a length of 10 μm at a magnification of ×300.